Weak microcavity effects in organic light-emitting devices

V. Bulović, V. B. Khalfin, G. Gu, and P. E. Burrows
Department of Electrical Engineering, Center for Photonics and Optoelectronic Materials, Princeton University, Princeton, New Jersey 08544

D. Z. Garbuzov
Sarnoff Corporation, Princeton, New Jersey 08542

S. R. Forrest
Department of Electrical Engineering, Center for Photonics and Optoelectronic Materials, Princeton University, Princeton, New Jersey 08544

(Received 24 March 1998)

We present an integrated classical and quantum-mechanical theory of weak microcavity effects in layered media that treats both radiative and waveguided modes. The electromagnetic field of radiative modes is determined using classical field quantization, with the transition probability into each mode given by Fermi's ''golden rule.'' We apply this theory to model the dependence of the electroluminescence spectral intensity and polarization of organic light-emitting devices (OLED's) on emission angle, organic layer thickness, and applied voltage. Light propagation in the OLED layers and the substrate is described by both ray and wave optics. Theoretical predictions are compared to experimental observations on single heterostructure, and multiple layer stacked red-green-blue OLEDs. Analysis of the polarization, spectral shape, and intensity of the electroluminescence spectrum in the forward-scattered half plane accurately fits the experimental data. The theory predicts, and the experimental measurements confirm, that the in-plane emission from conventional OLED structures is strongly TM polarized, and can be redshifted by as much as 60 nm with respect to the peak emission in the normal direction. Measurements coupled to our analysis also indicate that the efficiency of generating singlet excitons in aluminum *tris*(8-hydroxyquinoline) (Alq_3)-based OLED's is 5 ± 1 %, with a ~500-Å-thick Alq_3 layer corresponding to the highest external power efficiency. [S0163-1829(98)04532-9]

I. INTRODUCTION

Light generated by an organic light-emitting device (OLED) is due to the radiative recombination of excitons on electrically excited organic molecules. The radiative lifetime of these excited molecular states can be strongly influenced by the device structure. Since the thin dielectric molecular layers of an OLED are bounded by metallic electrodes and other reflective surfaces, this structure acts as an optical microcavity for the emitted radiation. The microcavity determines the electric-field mode distribution, thereby modifying the exciton spontaneous emission lifetime[1] and hence the quantum efficiency. This, in turn can modify the spectral width[2] and distribution of the emission intensity.[3] In optically pumped organic microcavity structures with reflective mirrors, lasing action has been observed.[4] However, even weak reflections in a conventional OLED structure are sufficient to form a microcavity that can significantly influence device luminescence properties.[5] Considering the ubiquity of microcavity effects in OLED's, it is important to describe them with a comprehensive theoretical model, coupled to an equally comprehensive set of experimental data, which is the focus of this study.

The earliest theoretical description of microcavity effects was presented by Purcell[6] who predicted the modification of the spontaneous emission rate for a dipole in a one-dimensional cavity. Since then, a number of studies[7–11] examined changes in the rate, spectrum, and directionality of emission of radiative dipoles in layered media using two different theoretical approaches: one classical and the other based on quantum mechanics.

The most complete classical picture was presented by Chance, Prock, and Sibley[9] where the radiating molecule is treated as a classical oscillating dipole. The radiation field is described by constructing a Green's function for the layered dielectric medium containing the oscillator, where the total radiative energy is calculated by integrating the Poynting vector in the forward scattered direction. This approach was shown to accurately describe the radiation of a dye molecule near a metal mirror for dye-metal distances as small as 100 Å.[9] More recently, the same theory was used to describe changes in exciton radiative lifetimes in luminescent, vacuum-deposited molecular organic thin films used in electrically pumped OLED's.[5] A similar classical treatment using wave optics and a transfer matrix formalism at the dielectric boundaries[12] was shown to agree with measured changes in the emission intensity with layer thickness,[5,13] and spectral narrowing in microcavity structures.[14] Classical wave optics applied to a Fabry-Pérot etalon was also shown to describe spatial variations in the emission intensity[15] and spectrum.[16]

In the quantum treatment, the electromagnetic field in a layered medium is represented by the sum of eigenmodes, where the transition probability into each of the modes is determined via Fermi's ''golden rule.'' This approach is convenient for structures with a large number of layers, and has

been successfully used in calculating the emission spectra of Al(Ga)As/GaAs (Refs. 10 and 11) vertical cavity surface-emitting lasers and light-emitting diodes. A shortcoming of this quantum-mechanical approach is that it does not account for nonradiative losses to the metal electrodes, or to absorption. However, it was shown by the Green's-function analysis[9] that nonradiative losses primarily affect the total rate of radiative emission, while only weakly influencing the electric field inside the microcavity.

For a full understanding and a convenient description of the complex radiation pattern observed for OLED's, a combination of both approaches is desirable. The quantum-mechanical description gives a simple form for the electric field within the microcavity, where Fermi's ''golden rule'' can be applied to predict transition rates. The numerically more involved classical (Green's function) treatment can then account for the rate of nonradiative energy losses to the metal electrodes and other materials used in the structure. In our theoretical treatment, we use this combination of the quantum and the classical pictures to completely describe the dependence of emission on angle and polarization. Additionally, waveguiding effects are modeled,[17,18] and their polarization dependence is described. Our theoretical predictions are compared to experimental measurements on conventional molecular organic single heterojunction OLED's,[19] as well as a significantly more complex stacked multicolor OLED (SOLED).[20] This approach accurately predicts the measured changes in the TE and TM radiation spectra with the change in emission angle and organic layer thickness. We model the in-plane emission, which is strongly TM polarized, red-shifted, and spectrally narrowed as compared to the surface normal emission, along with the change in the ratio of integrated surface-to-edge emission with the change in organic layer thickness and applied current. The agreement between experiment and theory allows us to suggest OLED structures that can result in enhanced emission in the forward-scattered direction. Finally, we compare the measured and predicted emission spectra of the three color-emissive elements in a complex, fourteen-layer SOLED as an example of the accuracy and versatility of this theoretical approach.

To our knowledge, this is the first complete theoretical treatment of changes in the exciton lifetime and the angle-dependent radiation spectra of dielectric structures that considers both radiation and waveguide modes, and their dependence on polarization. Differing from most other theoretical treatments that focus on strong microcavities, here we emphasize weak microcavity effects that dominate the performance of conventional OLED's.

This paper is organized as follows: In Sec. II, we describe the OLED structure and present a general theoretical description of waveguide and radiative modes in layered media for TE and TM polarized light. Experimental details of device fabrication and measurement are presented in Sec. III, and in Sec. IV the theoretical predictions are compared to experimental measurements. In Sec. V we apply this theory to understand the emission from a multicolor, multilayer stacked OLED. Conclusions are presented in Sec. VI.

II. THEORY

A. Archetype OLED structure

We apply our analysis to the OLED structure shown in Fig. 1. The device consists of an electron transporting (ETL) and electroluminescent (EL) layer of aluminum *tris*(8-hydroxyquinoline) (Alq_3) with a refractive index of $n_{Alq} = 1.72$, and a hole transporting layer (HTL) of 4, 4′-bis[*N*-(1-napthyl)-*N*-phenyl-amino] biphenyl (α-NPD) with $n_{NPD} = 1.78$. The bilayer structure typically has a total thickness of ~1000 Å. The organic materials are sandwiched between a 500-Å-thick Mg:Ag cathode with a 1000-Å-thick Ag cap, and a transparent, 1600-Å-thick indium-tin oxide (ITO) anode with $n_{ITO} = 1.8$. The entire structure is grown on a ~1-mm-thick glass substrate. The EL is generated within the weak microcavity formed by the highly reflective top metal electrode and a less reflective ITO/glass interface.

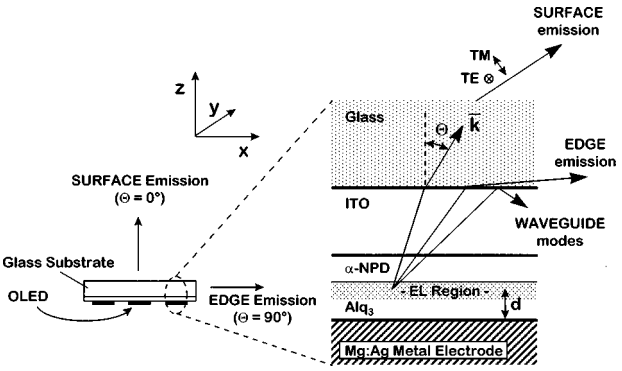

FIG. 1. Schematic diagram of a conventional OLED (left) along with the various radiative modes generated within the structure (right).

B. Exciton recombination processes

Electroluminescence is due to the radiative recombination of Frenkel excitons[21] within the organic layers. The excited molecular state can undergo radiative transitions at rate W_R^0 and nonradiative transitions such as internal conversion and intersystem crossing, at rate W_{NR}^0. By measuring the fluorescence quantum efficiency of emission η_0 for a thick slab of the radiative organic layer,[17] the influence of microcavities can be ignored and the *intrinsic* rates, $W_R^0 \equiv W_0$ and W_{NR}^0, are determined via

$$\eta_0 = W_0/(W_0 + W_{NR}^0). \tag{1}$$

Within a microcavity, the exciton can transfer its energy either to the externally radiated modes, or to the waveguide modes propagating in the plane of the structure with rates, W_R and W_{wg}, respectively. Furthermore, a fraction of the electromagnetic radiation is lost to the metal cathode via nonradiative dipole-metal energy transfer, and excitation of surface plasmons. The energy transfer rates for these two processes are given by $W_{D\text{-}M}$ and W_{SP}, respectively. Assuming that the placement of an exciton inside the microcavity minimally affects the nonradiative transition rate, then $W_{NR} = W_{NR}^0$. In this case, the total recombination rate of an exciton in the microcavity is

$$W_{TOT} = W_R + W_{wg} + W_{D\text{-}M} + W_{SP} + W_{NR}. \tag{2}$$

We now discuss all of these processes, first presenting the derivation of the rate equations for radiation modes.

C. Radiation modes

The one-dimensional electric field distribution of a radiation mode along the normal, $\hat{z}$ direction, in an OLED is found using Maxwell's equations that satisfy standard boundary conditions across the various dielectric layer interfaces. To simplify the analysis, the metal cathode is initially treated as a perfect reflector. Propagation in the glass substrate is determined using ray optics since the substrate thickness is much larger than the wavelength of light. Interference due to reflections from the two substrate surfaces can thus be neglected.

Each radiation mode can be described by a wave vector $\mathbf{k}$ representing a sum of incoming and outgoing plane waves. The radiation intensity emitted by an exciton into an eigenmode $\mathbf{k}$ is proportional to the transition probability rate into this mode given by Fermi's ''golden rule:''

$$dW = \frac{2\pi}{h} |F_{mn}|^2 \delta(\mathcal{E}_n - \mathcal{E}_m - h\nu). \tag{3}$$

Here, F_{mn} is the electric dipole matrix element, $\langle n|\boldsymbol{\mu}\cdot\mathbf{E}(\mathbf{k},z)|m\rangle$, where $\boldsymbol{\mu}$ is the dipole moment and $\mathbf{E}$ is the electric field for mode $\mathbf{k}$ at the position z. $\mathcal{E}_m$ and $\mathcal{E}_n$ are energies of the initial ($|m\rangle$) and final ($|n\rangle$) exciton states, while ν is the frequency of the emitted photon. Summing over all $\mathbf{k}$, we can determine the total radiative dipole lifetime. For an amorphous material, averaging over all dipole moment orientations is also required.

For the archetype structure of Fig. 1, we derive transition rates into TE modes polarized in the plane of the substrate, and the TM modes. For radiative TE modes, it is convenient to express the transition rate through E_Y, while for the radiative TM mode it is more convenient to use the H_Y component of the magnetic field.[12] Here, the subscript Y refers to the in-plane component of the particular field, and both E_Y and H_Y represent ratios of the fields at the position of the exciton to the fields in free space outside the layered structure. Determining the electromagnetic field in the layered structure and applying Eq. (3), we obtain the following expressions for the radiation rate into solid angle, $d\Omega$, within the glass substrate:

For TE modes:

$$dW_R^{\mathrm{TE}} = W_0 \frac{1}{4\pi} \frac{n_G}{n_M} |E_Y|^2 d\Omega; \tag{4}$$

for TM modes:

$$dW_R^{\mathrm{TM}} = W_0 \frac{1}{4\pi} \left[\frac{n_G^3}{n_M^5} \sin^2\Theta |H_Y|^2 + \frac{n_G}{n_M^5 k_0^2} \left| \frac{dH_Y}{dz} \right|^2 \right] d\Omega. \tag{5}$$

Here, n_G is the refractive index of the glass substrate, n_M is the refractive index of the organic layers (assumed for simplicity to be approximately equal for both the ETL and HTL), Θ is the angle between $\hat{z}$ and $\mathbf{k}$ in the substrate, and $k_0 = 2\pi/\lambda$ is the wave vector in free space at wavelength λ. These expressions implicitly depend on the wavelength of the emitted light and the spatial position of the radiating dipole (given by distance d from the metal electrode; see Fig. 1). Furthermore, E_Y and H_Y also depend on Θ. To obtain the spatial distribution of radiation modes in air, refraction at the glass/air boundary has to be taken into account. For $\Theta = 0°$, Eqs. (4) and (5) are equivalent, as expected.

Although the above derivation assumes lossless media and lossless mirrors, Eqs. (4) and (5) can easily be extended to determine the radiation pattern in the presence of losses.[9] The quantum efficiency for radiative emission is given by

$$\eta_R = W_R / W_{\mathrm{TOT}}, \tag{6}$$

where the detailed influence of the nonradiative transitions ($W_{D\text{-}M}$ and W_{SP}) on the emission spectrum depends on the dispersion in the complex refractive index of the metal electrode. Typically, for dipole-electrode distances greater than a few hundred angstroms, the dipole-metal nonradiative energy transfer and excitation of surface plasmons minimally affects the electric field distribution within the microcavity and the shape of the emission spectrum. We therefore also use Eqs. (4) and (5) in the presence of nonradiative losses.

To obtain the radiation spectrum within solid angle, $d\Omega$, of a luminescent source embedded in a layered structure, we need to know its intrinsic radiation spectrum along with its spatial distribution within the EL layer. For each wavelength and distance d, we can then calculate Eqs. (4) and (5), weighted for the relative spectral intensities of the intrinsic radiation spectrum, and the exciton density within the EL layer.

As is generally the case, we assume that all radiation originates from the excitons in the EL layer. After being generated at the ETL/HTL interface, excitons diffuse into the EL layer, reaching a steady state, exponentially decaying distribution with characteristic width L_{REC}, that is on the order of the exciton diffusion length L_D (typically $\sim$200 Å for Alq_3).[22] An accurate description of L_{REC} would take into account the spatial profile of the density of injected carriers in the ETL as a function of the voltage applied across the OLED. As will be shown below, however, we observe that this effect produces minimal correction to the final result, and therefore we assume $L_{\mathrm{REC}} = 200$ Å throughout our calculations.

D. Waveguide modes

The light generated in the EL layer can reach the ITO/glass interface where it is either refracted into the glass substrate contributing to radiation modes, or it is reflected back into the OLED structure, contributing to waveguide modes. This process is governed by the angle and polarization of the light incident at the ITO/glass interface.

The waveguide modes are guided in both the ITO and the organic layers. A $\sim$2500-Å-thick asymmetric ITO/organic waveguide can support up to five TE and TM eigenmodes at $\lambda = 520$ nm (corresponding to the peak emission wavelength of Alq_3). The total electromagnetic field intensity does not vary strongly over the waveguide thickness, since TE modes have minima near the metal electrode, where TM modes are at a maximum. Therefore, the rate of energy transfer from the excited dipole into the waveguide modes (W_{wg}) is only a weak function of the dipole position.

To calculate the transition probability into the waveguide modes, we use the same analysis as for the radiative modes. The only difference is in the normalization of the eigenmodes, since $\mathbf{k}$ is now a two-dimensional wave vector in the

plane of the structure. The density of states for the guided modes is $A\,d^2k/(2\pi)^2$, where A is the unit area. To determine the energy density of states, we need to know the group velocity, $\boldsymbol{\nu}=\mathbf{S}/U$, where $\mathbf{S}$ is the energy flux per unit length perpendicular to the propagation direction, and U is the energy density per unit area,[23] such that $UA=h\nu$. Hence, to obtain $\boldsymbol{\nu}$, it is only necessary to calculate the Poynting vector of the guided waves. A benefit of this approach is that we do not need to calculate the amplitude of the guided waves, since in the final expression the electric field amplitude appears simultaneously in the numerator and the denominator. After averaging over all directions of the transition dipole moment, we obtain for the transition probability into waveguided TE and TM modes:

TE modes:

$$W_{\mathrm{wg}}^{\mathrm{TE}}=W_0\,\frac{\pi}{2n_Mk_0}\,\frac{|E_Y|^2}{\int|E_Y|^2dz}; \tag{7}$$

TM modes:

$$W_{\mathrm{wg}}^{\mathrm{TM}}=W_0\,\frac{\pi}{2n_Mk_0}\,\frac{(n_G^2/n_M^2)|H_Y|^2+(1/n_M^4k_0^2)|dH_Y/dz|^2}{\int(|H_Y|^2/n_i^2)dz}. \tag{8}$$

The integrals in the denominators of Eqs. (7) and (8) are over the transverse distribution of the guided mode, where n_i is the refractive index of the corresponding layer (organic, ITO, or glass). In this case the fields are not normalized as in Eqs. (4) and (5). The radiation pattern of waveguided modes is isotropic in the plane of the structure.

To calculate the total-energy transition rate into the waveguided modes, we first calculate the number of guided modes supported by the OLED structure for each of the wavelengths in the emission spectrum.[23] The transition probability into the waveguide modes is then calculated for each allowed wave vector as a function of dipole position d using Eqs. (7) and (8).

E. Nonradiative energy transfer and surface plasmons

Nonradiative energy transfer is due to the near field interaction of the radiative dipole with the lossy metal electrode, and strongly depends on their relative positions. A second process of coupling to surface plasmon modes of the metal electrode occurs for both lossy and lossless electrodes of metals with finite negative dielectric constants. This term decreases exponentially with distance from the electrode.

Our simple theoretical model does not take into account these losses to the metal electrode. They can, however, be described classically by constructing the Green's function for the electric field inside the layered medium,[9] using the complex dielectric susceptibility of the metal layer. In Fig. 2 we use this method to calculate the dependence of $W_{\mathrm{TOT}}-W_{\mathrm{NR}}$ on distance d from the Mg:Ag cathode in an Alq_3/α-NPD OLED with a combined ITO and organic layer thickness of 2500 Å. High values of $W_{\mathrm{TOT}}-W_{\mathrm{NR}}$ near the electrode are due to the increase in $W_{D\text{-}M}$. The average of rates for x-, y-, and z-oriented dipoles is in agreement with earlier measurements of exciton recombination times in the vicinity of a metal interface.[1] The value of $W_{\mathrm{TOT}}-W_{\mathrm{NR}}$ quickly decreases with distance, and approaches W_0 at d $=600-800$ Å. At larger distances, $W_{\mathrm{TOT}}-W_{\mathrm{NR}}$ changes by no more than $\pm 0.5W_0$, due to the combined effects of interference of radiative modes and the redistribution of the waveguide mode fields.

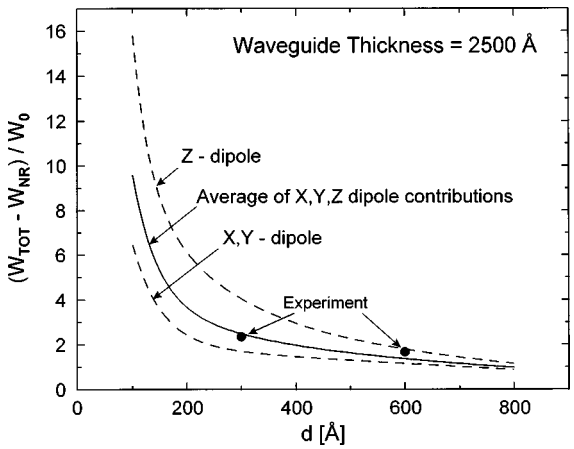

FIG. 2. Calculations of the total rate of energy transfer (W_{TOT}) from an Alq_3 exciton into various radiative (W_R, W_{wg}) and nonradiative ($W_{D\text{-}M}$, W_{SP}) processes (excluding internal-conversion and intersystem crossing, W_{NR}) as a function of the exciton distance from the metal electrode (d). The total waveguide thickness was held constant at 2500 Å. The experimental measurements of Ref. 1 are also shown.

The presence of the metal electrode can strongly affect the ratio of the total normal-to-edge (in-plane) emission of a radiative dipole. For small d, the metal electrode mirror suppresses the dipole radiation in the vertical direction since the boundary conditions at the surface of an ideal reflector require the absence of the tangential component of the electric field. However, the change in the total radiation probability into both the waveguide and radiation modes is much less affected by proximity to the electrode since the electric field of the TM modes has its maximum near the mirror.

III. MEASUREMENT TECHNIQUE AND SAMPLE PREPARATION

The theoretical predictions were tested by measuring the photoluminescence and electroluminescence spectra of a series of Mg:Ag/Alq_3/α-NPD/ITO OLED's with different organic layer thicknesses. The detection angle Θ was varied from 0° (emission normal to substrate) to 90° (edge emission). A broad area (12×12 mm^2) silicon photodetector was used to measure the integrated spectral intensity. For polarization-sensitive measurements, a linear polarizer was placed in front of the detector. The EL and PL spectra were collected by a single lens with a full angle acceptance cone of 15°, and focused onto the entrance slit of a 0.275-m single grating spectrograph with a 0.5-Å spectral resolution using a charge-coupled device (CCD) array detector. A pulsed (40 Hz) nitrogen laser was used as the $\lambda=337$ nm photoexcitation source in the PL measurements.

The OLED's were grown by high vacuum (10^{-6} Torr) thermal evaporation onto the surface of a precleaned, ITO-coated (1600-Å-thick layer) glass substrate using techniques described previously.[22] A 12×12 mm^2 substrate was used with all of the edge facets polished to reduce scattering. The

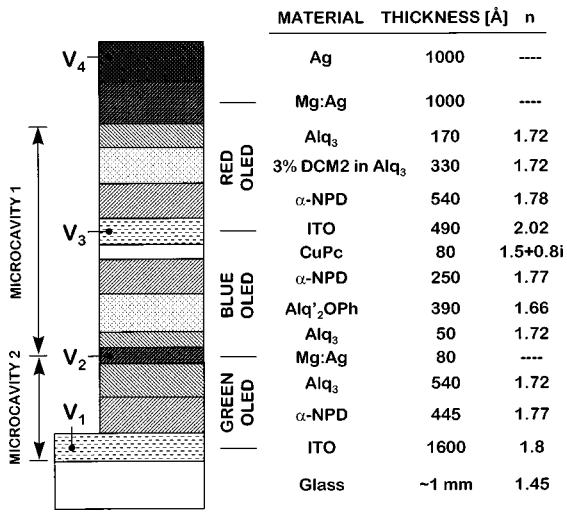

FIG. 3. Schematic diagram of a stacked OLED, listing materials, thicknesses, and refractive indices of the layers.

organic materials were layered as in Fig. 1 where a 500-Å-thick α-NPD HTL was first deposited, followed by 200 Å to 950 Å of Alq_3, which served as both EL and ETL. For one set of samples, a 100-Å-thick cap layer of 4, 4′-di(*N*-carbazole)biphenyl (CBP) was grown on the Alq_3 surface. The cathode, consisting of a 500-Å-thick, 25:1 Mg:Ag alloy and 1000-Å-thick Ag layer, was then deposited through a shadow mask defining 1-mm-diameter circular electrodes. The set of samples used in Fig. 12 employed a 50-Å-thick copper phthalocyanine (CuPc) layer grown on top of the ITO, and a 350-Å-thick α-NPD HTL, to reduce the device operating voltage. For PL samples, the HTL and CuPc layer was omitted. Layer deposition rates ranged from 1–5 Å/s.

For the three color emitting, stacked OLED discussed in Sec. V, the first ITO layer was photolithographically patterned to form the electrode V_1 on top of which the remainder of the device structure was grown through a set of six shadow masks, as described elsewhere.[20] The completed structure with layer thicknesses and their corresponding refractive indices is shown in Fig. 3. The SOLED contains a conventional α-NPD/Alq_3 green emitting device with a semitransparent Mg:Ag cathode (V_2) on top of which is grown a bis-(8-hydroxy)quinaldine aluminum phenoxide ($Alq_2'OPh$)/α-NPD blue organic inverted LED (OILED) (Ref. 24) with a CuPc ''protection layer'' at the anode. The OILED anode (V_3) is an ITO layer grown by low-power sputter deposition. This layer simultaneously serves as the anode of the red emitting device. The red OLED consists of an α-NPD HTL, an Alq_3 luminescent layer 3% doped with an organic dye DCM2, an Alq_3 contact layer, a Mg:Ag cathode (V_4), and a Ag cap layer.[25] Red light emission originates from DCM2 molecules that are excited via Förster energy transfer from Alq_3. The 1000-Å-thick Ag cap-layer inhibits top electrode oxidation. Electrodes V_1, V_2, V_3, and V_4 are independently addressed, allowing for independent intensity control of the green, blue, and red emissive elements.

IV. RESULTS AND DISCUSSION

A. Dependence on layer thickness

The contribution of the metal electrode to microcavity effects in the OLED structure is evident from Fig. 4, where

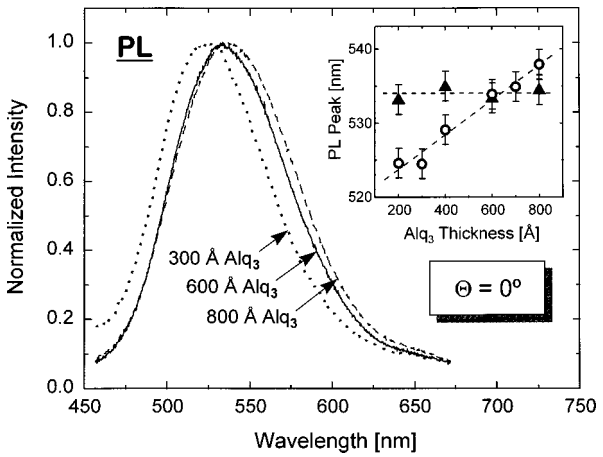

FIG. 4. Photoluminescence spectra at $\Theta = 0°$ of three devices with the following structure: glass substrate, 1600-Å ITO, *xxx*-Å Alq_3, 500-Å Mg:Ag, 1000-Å Ag. Inset: Peak PL emission wavelength as a function of Alq_3 layer thickness for structures with (open circles) and without (solid triangles) metal cathodes.

the PL spectra at $\Theta = 0°$ of a series of devices of different thicknesses of Alq_3, with and without a reflective metal electrode, are compared. The Alq_3 layer was excited by a $\lambda = 337$ nm, 1-mm-diameter spot incident through the substrate, positioned beneath the metal electrode. The 15-nm shift in the peak PL emission wavelength with a 200–800-Å change in Alq_3 thickness (open circles in the inset of Fig. 4) is attributed to reflections from the cathode that result in the pronounced microcavity effects. This is supported by the PL spectra collected in regions not covered by the cathode, showing no peak shift (solid triangles in the inset, Fig. 4).

Similarly, the spectral shape of the $\Theta = 0°$ EL emission is also influenced by the thickness of the Alq_3 layer, which determines both the length of the microcavity and the position of the OLED active region within the microcavity. A 20-nm redshift in peak EL emission is observed in Fig. 5

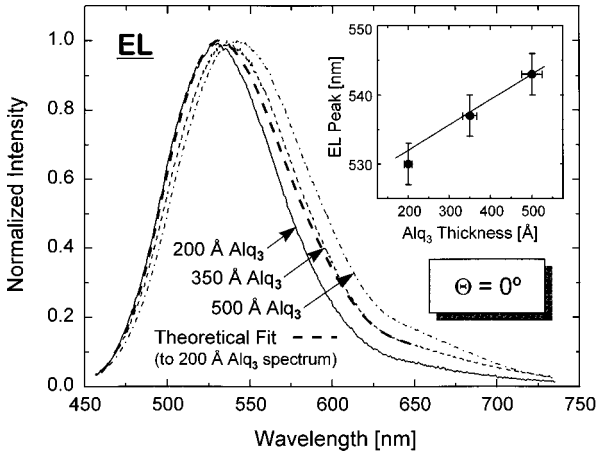

FIG. 5. Electroluminescence spectra at $\Theta = 0°$ of three OLED's with the following structure: glass substrate, 1600-Å ITO, 500-Å α-NPD, *xxx*-Å Alq_3, 500-Å Mg:Ag, 1000-Å Ag, and with Alq_3 layer thickness of 200, 350, and 500 Å. The theoretical fit (bold, dashed line) to the electroluminescence spectrum at $\Theta = 0°$ for the OLED with a 200-Å-thick Alq_3 layer (solid line) is shown. Inset: Peak EL emission as a function of Alq_3 layer thickness compared to theoretical predictions.

when the Alq_3 thickness is increased from 200 to 500 Å.

To compare these experimental observations to our theoretical model, we modify the *intrinsic* Alq_3 emission spectrum according to Eqs. (4) and (5) to fit the spectra at different layer thicknesses. At $\Theta = 0°$, Eqs. (4) and (5) are equal and can be used to find W_0 in terms of W_R. The intrinsic spectrum is determined from a device with the thickest (500 Å) Alq_3 layer, and is used as the basis for all theoretical fits in Figs. 5 through 12. The theoretical prediction (shown by the dashed line in Fig. 5) for the $\Theta = 0°$ EL emission of a device with a 200-Å-thick Alq_3 layer is in reasonable agreement with the experimental measurements. The minor differences in the measured and predicted spectral width are primarily due to the nonzero acceptance cone of the spectrograph. The peak EL wavelength for this and other Alq_3 thicknesses along with the theoretical prediction (solid line) is shown in the inset of Fig. 5. Comparing Figs. 4 and 5, we find that both the trend and magnitude of the spectral shifts are similar whether the emission is via EL or PL. This is strong evidence that microcavity effects induced by the reflective metal electrode are responsible for the shifts in both cases.

B. Dependence on emission angle and wavelength

The angular dependence of both the TE and TM polarized EL spectra of an OLED with a 500-Å-thick Alq_3 layer is shown in Fig. 6(a). These spectra were obtained by placing the flat face of a glass hemisphere in contact with the substrate, wetting the gap between the lens and the substrate with an index-matching fluid to avoid reflections. The OLED was positioned at the center of radius of the hemispherical lens. By this means, light refraction at the lens/air interface was avoided, and the angular distribution of radiation in air was identical to that in the glass substrate. The experimental measurement (solid lines) and the theoretical prediction (dashed lines) for TE and TM spectra at $\Theta = 65°$ are shown in Fig. 6(b). The theoretical predictions are in equally good agreement for other directions as evident in Fig. 7(a) where the change in the peak wavelength of both TE and TM emission as a function of Θ is compared to the theory (solid and dashed line fits). Figure 7(b) shows the ratio of the TM to TE mode intensity as a function of angle, which is also in agreement with calculations shown by the solid line. The angular dependence of the EL spectra is a strong function of the device layer thickness and refractive index. Hence, these fits provide a rigorous test of validity of the analysis.

Especially interesting is the spectral emission from the substrate edge at $\Theta \sim 90°$. This radiation is observed to be nearly completely TM polarized, and is narrowed and redshifted with respect to the spectrum in the normal direction. Figure 8(a) shows the $\Theta \sim 90°$ TM emission spectra as a function of Alq_3 thickness for the same series of OLED's as studied in Fig. 5(a). For all devices, the spectral full width at half maximum is 50 nm, as compared to 100 nm at $\Theta = 0°$. A 30 nm redshift occurs when the Alq_3 layer thickness increases from 200–500 nm. Previous measurements of the $\Theta \sim 90°$ emission spectra of an Alq_3 sandwich structure with Au:Ag and Mg:Ag metal electrodes[26] show a shift in peak emission with the change in the organic layer thickness. The

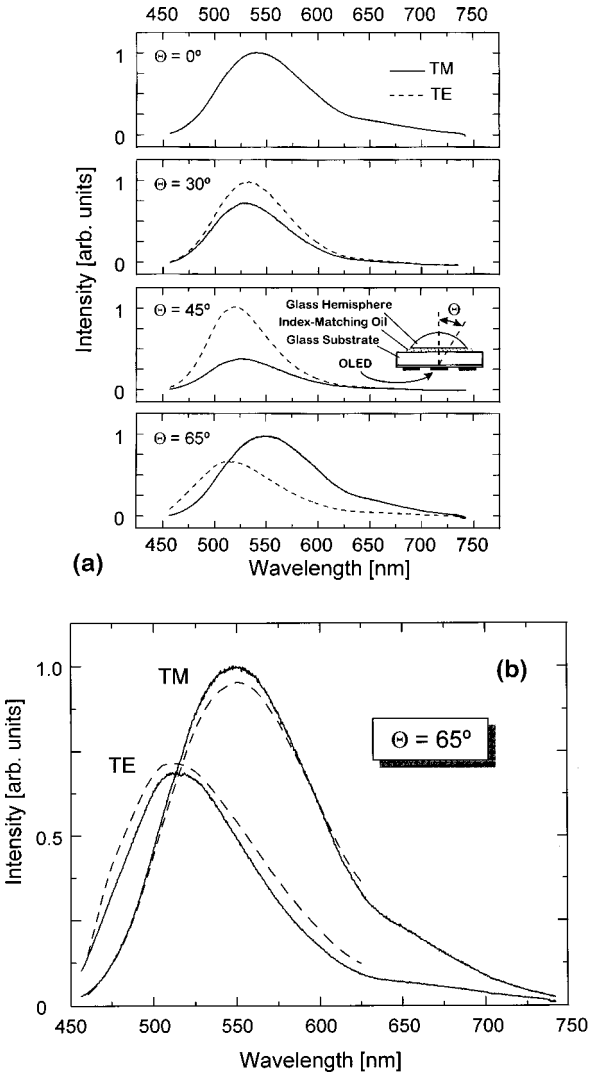

FIG. 6. (a) TE and TM electroluminescence spectra as a function of exit angle, Θ, for an OLED with the following structure: glass substrate, 1600-Å ITO, 500-Å α-NPD, 500-Å Alq_3, 500-Å Mg:Ag, 1000-Å Ag. (b) Theoretical fit of the TE and TM spectra at $\Theta = 65°$.

observed shift in that earlier work can be associated with the change in waveguide modes with layer thickness.

In conventional OLEDs, we note that the $\Theta \sim 90°$ directed light can originate from *either* radiative *or* waveguide modes. The contribution to these spectra of the waveguided light was investigated by estimating and measuring losses in the ITO/organic waveguide core. In modeling the electric field profile of the waveguide modes, we note that the mode tail is absorbed by the metal electrode that forms one of the waveguide boundaries. The strong metal absorption contributes to propagation losses that are estimated to be $\sim 1000\ cm^{-1}$. This loss is obtained using the waveguide equation for the propagating mode with the complex dielectric constant of the metal, along with the fraction of the evanescent mode intensity coupled into the electrode. Such high losses imply that virtually all of the $\Theta \sim 90°$ emission originates from the radiative modes. This conclusion is in agreement with edge emission measurements of OLED's grown on substrates with a patterned ITO layer, where the ITO does not extend to the edge of the glass substrate, as shown in the

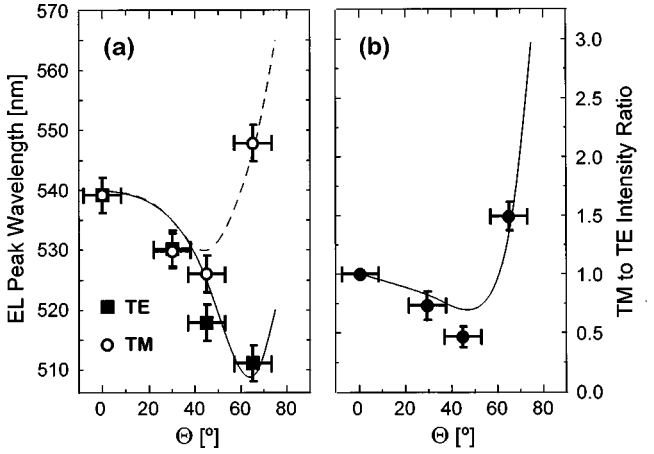

FIG. 7. Measured (a) peak TE and TM emission wavelength and (b) TE to TM integrated intensity ratio vs Θ of the OLED from Fig. 6 (symbols), compared to calculations (solid and dashed lines).

experimental configuration illustrated in the inset of Fig. 8(b). In this case, the waveguide modes emerge from the end of the ITO layer, while the radiative modes exit from the edge of the glass substrate. The cathode was positioned from 1 to 3 mm from the edge of the ITO layer, which in turn was 2 mm from the edge of the glass substrate. Even for the shortest ITO-to-edge distance of 1 mm, no emission from the ITO layer edge was observed, implying no contribution from the waveguide modes to the edge emission. When a thick absorptive organic layer was grown over the ITO layer edge in order to attenuate the waveguide mode contribution to the edge emission spectrum, the resulting spectral shape, polarization, and intensity were unchanged. From this we conclude that the contribution of waveguided light to the edge emission is negligible due to high propagation losses.

The edge emission spectra are, therefore, primarily due to radiative modes whose polarization dependence and spectral shape are explained as follows: The cos Θ dependence of the Lambertian distribution of the emission suggests only a weak intensity at $\Theta \sim 90°$. Indeed, TE polarized, $\Theta \sim 90°$ emission is not observed. However, for TM polarization, the $\Theta \sim 90°$ emission is enhanced due to the Fabry-Pérot resonance condition inside the waveguide core, where the electric field (E_Y) is proportional to $1/D$ with

$$D = 1 - R_1 R_2 \exp(2ik_\perp t). \tag{9}$$

Here, R_1 and R_2 are the reflectivities of the cathode and the glass/ITO interface, $k_\perp$ is the component of the propagation vector normal to the substrate, and t is the waveguide core thickness. In this case, R_1 and R_2 differ for TE and TM modes. At the cutoff frequency of the waveguide, the normal component of the propagating mode wave vector is $k_\perp^c$, then wave vectors with $k_\perp = k_\perp^c - \delta k_\perp$ will contribute to $\Theta \sim 90°$ radiative emission. In general, for certain values of $k_\perp = k_\perp^{wg}$, the characteristic equation for waveguide modes given by $D = 0$ is satisfied, and a mode with $k_\perp^{wg}$ propagates within the waveguide. Therefore, if $k_\perp^{wg} \sim k_\perp^c$, then $D \sim 0$ for $k_\perp = k_\perp^c - \delta k_\perp$, resulting in a large E_Y for this $k_\perp$, and a non-negligible $\Theta \sim 90°$ emission. For our structure, the observed maximum in the edge emission spectrum coincides with the cutoff wavelength of the first TM mode. With the

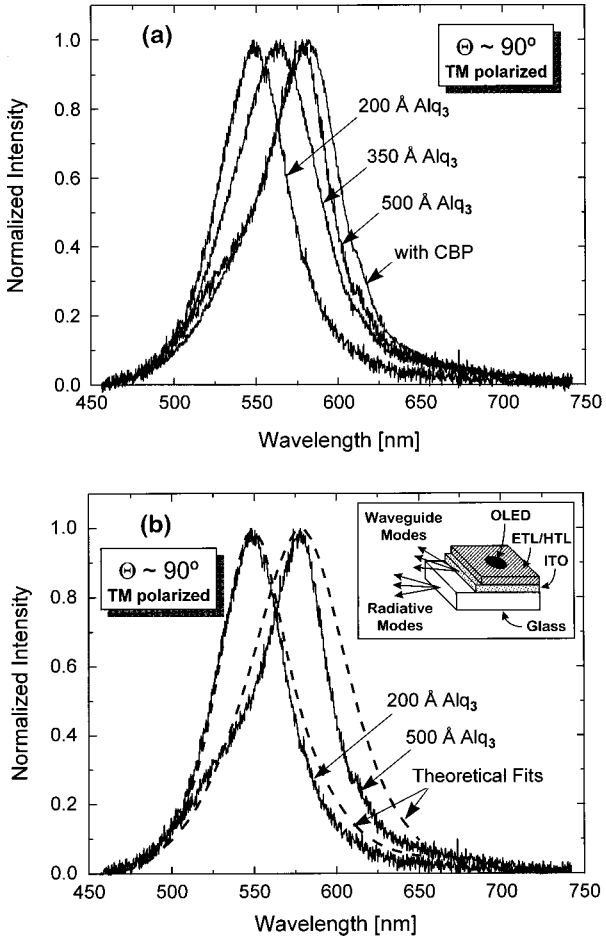

FIG. 8. (a) Edge-emitted electroluminescence spectra at $\Theta \sim 90°$ of three OLED's with the following structure: glass substrate, 1600-Å ITO, 500-Å α-NPD, *xxx*-Å Alq_3, 500 Å Mg:Ag, 1000-Å Ag, and Alq_3 layer thicknesses of 200, 350, 425, and 500 Å, and an OLED with the following structure: glass substrate, 1600-Å ITO, 500-Å α-NPD, 450-Å Alq_3, 100-Å CBP, 500-Å Mg:Ag, 1000-Å Ag. (b) Theoretical fit (dashed line) to the $\Theta \sim 90°$ electroluminescence spectrum (solid line) of OLED's with a 200-Å- and 500-Å-thick Alq_3 layer. Inset: Structure of the device used to investigate the contribution of waveguide modes to the radiation spectrum.

decrease in Alq_3 layer thickness, the cutoff wavelength is blueshifted, which explains the observed position in the $\Theta \sim 90°$ peak EL emission [Fig. 8(a)].

For $\Theta \sim 90°$ emission, the measured EL spectrum is very sensitive to small changes in the angle of observation. Therefore, in Fig. 8(b) the calculated radiative mode spectra for TM polarized radiation (dashed lines) are averaged over the 8° median angle of the detector acceptance cone. The agreement between the experimental and calculated spectra is apparent. The luminescence peak and long-wavelength cutoff are sensitive to the waveguide thickness, while the spectral width is dependent on the detection angle. The estimated intensity of the TE polarization is nearly two orders of magnitude smaller than shown for TM modes.

We also considered the possibility that the edge emission is due to radiative recombination of excitons within a thin damaged layer of Alq_3 located near to the metal electrode. The damage may occur during metal deposition,[24] producing molecular fractions or other compounds that redshift the

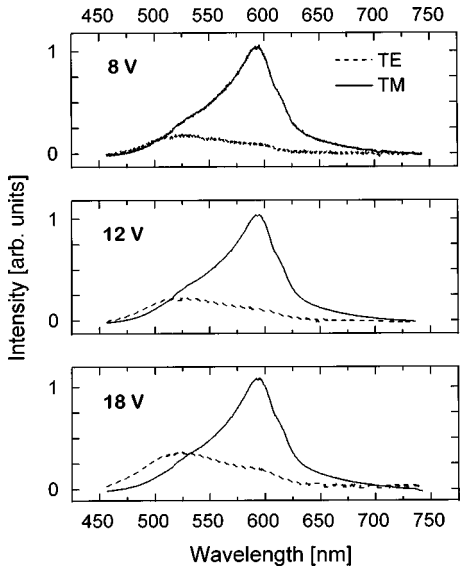

FIG. 9. Edge-emitted TE and TM electroluminescence spectra at $\Theta \sim 90°$ direction of an OLED with the following structure: glass substrate, 1600-Å ITO, 500-Å α-NPD, 500-Å Alq_3, 500-Å Mg:Ag, 1000-Å Ag at three different applied biases of 8 V (corresponding to $I \sim 10^{-3}$ A/cm^2), 12 V ($I \sim 10^{-1}$ A/cm^2), and 18 V ($I \sim 10$ A/cm^2).

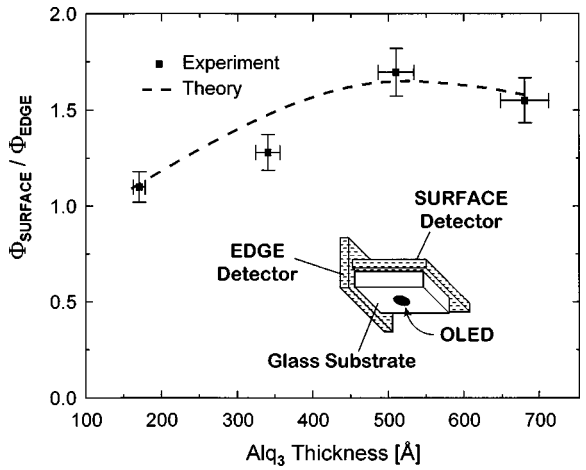

FIG. 10. Ratio of EL intensities in the direction normal to the substrate face to that emitted from the edge of the substrate ($\Phi_{surface}/\Phi_{edge}$) of four OLED's with the following structure: glass substrate, 1600-Å ITO, 500-Å α-NPD, *xxx*-Å Alq_3, 500-Å Mg:Ag, 1000-Å Ag, and Alq_3 layer thicknesses of 170, 340, 510, and 680 Å, compared to the theoretical prediction (dashed line) discussed in text. Inset: Experimental setup used to obtain data in the figure.

spectral emission. The immediate proximity to the metal electrode would quench the $\Theta = 0°$ dipole radiation in the damaged layer, thereby modifying only the $\Theta \sim 90°$ spectrum. To prevent formation of such a damaged layer, a 100-Å-thick nonemissive, electron injecting CBP cap layer[27] was grown on top of the Alq_3 prior to electrode deposition. The edge spectrum of the CBP-capped OLED [Fig. 8(a)] is similar to that of uncapped devices, although it too is somewhat redshifted since the waveguide thickness is further increased by the CBP layer. The existence of a damaged Alq_3 layer is thus not necessary to explain the observed spectral shifts.

We further consider the possibility that the spectrally narrow edge spectrum can be attributed to stimulated emission. However, no change in the spectral shape (Fig. 9) was observed as the voltage across an OLED with a 500-Å-thick Alq_3 layer was changed from 8 V (corresponding to a current of $I \sim 10^{-3}$ A/cm^2) to 18 V ($I \sim 10$ A/cm^2). The broad emission spectrum collected over the whole substrate edge exhibited no spectral narrowing, although there was a 10^4-fold linear increase in the output intensity with current, clearly indicating the lack of optical gain associated with stimulated radiation. With the increase in voltage, an increase in TE relative to TM intensity was observed, presumably due to light scattering in the structure.

We next compared the external efficiency for the radiation emitted normal to the substrate with that from the vertical edge facets. Earlier studies on shaped glass substrates suggested that by redirecting the edge-emitted light, the substrate normal emission can be enhanced by as much as $(90 \pm 20)\%$.[18] To investigate this effect, the total integrated EL emission through the surface and the edge facets of the OLED glass substrate was measured using the method shown in the inset of Fig. 10. Here, two silicon photodetectors simultaneously collected the radiation from two device surfaces. Figure 10 shows the ratio of measured light intensities from the substrate surface ($\Phi_{surface}$) (collected by the ''surface detector'') to that from its edges (Φ_{edge}) (collected by the ''edge detector'' and multiplied by four), as a function of Alq_3 layer thickness (α-NPD thickness $= 500$ Å). To calculate the ratio of the surface-to-edge emission, we integrate Eqs. (4) and (5) over both wavelength and solid angle. All radiation into the waveguide modes is absorbed as discussed above, while in the absence of scattering the light that undergoes total internal reflection at the glass/air interface can only be emitted through the edge facets. The absorption of radiative modes by ITO is negligible in our experiment, where the 12×12-mm^2 glass substrate is ~ 1 mm thick. For a glass refractive index of 1.45, 10%–20% of the total radiative intensity is trapped in the glass substrate by total internal reflection. In the fit of Fig. 10 (dashed line), we assume that the trapped radiation is divided equally between the substrate normal and edge emission. From these measurements, it is clear that by redirecting the edge-emitted light, the substrate surface emission can indeed be enhanced by 70% to 90%, in agreement with previous studies.[18]

Figure 11(a) shows the decrease in $\Phi_{surface}/\Phi_{edge}$ with increasing drive current for a device with a 510-Å-thick Alq_3 layer. It is reasonable to expect that with the increase in carrier injection, the width of the recombination region inside the Alq_3 layer also increases. Assuming that the radiating dipoles are exponentially distributed away from the HTL/ETL interface over a characteristic length, L_{REC}, then $\Phi_{surface}/\Phi_{edge}$ can be calculated by integrating Eqs. (4) and (5) over layer thickness, wavelength, and solid angle. From these calculations we obtain the relationship between L_{REC} and $\Phi_{surface}/\Phi_{edge}$ also plotted in Fig. 11(a) (top axis). Combining the two plots of Fig. 11(a), the dependence of L_{REC} on drive current I is determined and plotted in Fig. 11(b). An increase in the number of injected carriers increases L_{REC}, until at large I, $L_{REC} \rightarrow \infty$, implying a flat exciton distribution throughout the Alq_3 layer. The decrease in the surface emission with increasing L_{REC} is then due to a shorter average

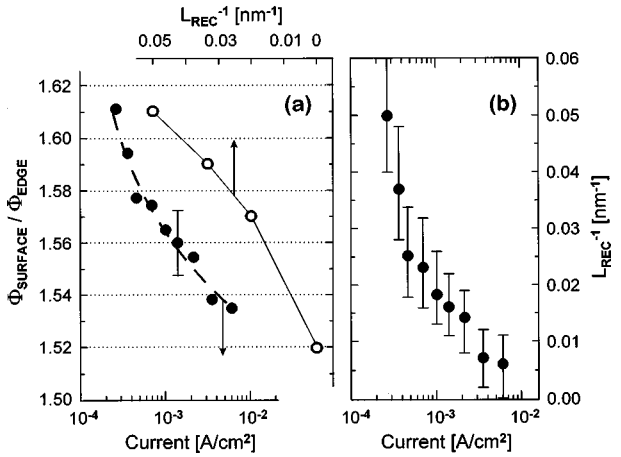

FIG. 11. (a) The $\Phi_{\text{surface}}/\Phi_{\text{edge}}$ ratio as a function of current (I) though an OLED with a 510-Å-thick Alq_3 layer. The calculated $\Phi_{\text{surface}}/\Phi_{\text{edge}}$ ratio as a function of the exciton recombination width, L_{REC}, is also shown. (b) Measured dependence of L_{REC} on the drive current.

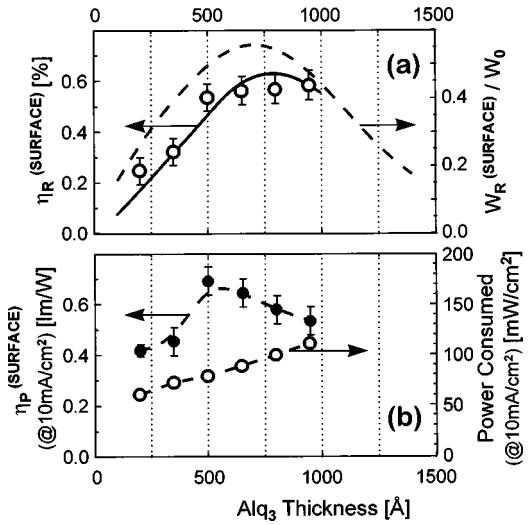

FIG. 12. (a) Calculated rate of energy transfer to the radiative modes emitted from the surface, $W_R^{(\text{surface})}$ (dashed line). Also shown are the calculated (solid line) and measured (symbols) surface emitted radiative efficiencies, $\eta_R^{(\text{surface})}$, as a function of Alq_3 layer thickness. (b) Measured OLED power consumption at the drive current of 10 mA/cm^2 (open circles), and power efficiency, $\eta_P^{(\text{surface})}$ (solid circles), of an OLED with the following structure: glass substrate, 1600-Å ITO, 50-Å CuPc, 350-Å α-NPD, *xxx*-Å Alq_3, 500-Å Mg:Ag, 1000-Å Ag.

distance between a radiating dipole and the metal electrode. As discussed earlier, for small d, the metal electrode mirror suppresses the dipole radiation in the vertical direction (cf. Fig. 2). Therefore, the change in the $\Phi_{\text{surface}}/\Phi_{\text{edge}}$ with increasing current in Fig. 11(a) can be ascribed to the increase in L_{REC}. We note that the error in the derived value of L_{REC} can be substantial due to its sensitivity to small changes in $\Phi_{\text{surface}}/\Phi_{\text{edge}}$ from device to device. However, a trend of increasing L_{REC} with I is apparent for all devices investigated.

C. Optimizing radiative efficiency

In order to maximize the radiative emission and power efficiency of OLED's, we calculated the dependence of the output coupling on a number of device parameters such as Alq_3, α-NPD, and ITO thickness and refractive index, by averaging Eqs. (4) and (5) over output angle and wavelength. To maximize external efficiency (and hence the rate of radiative transitions), the exciton must be at the antinode of a radiation mode. For the direction normal to the substrate, radiation modes have nodes near to the metal electrode. Therefore, at the peak wavelength of Alq_3 luminescence ($\lambda = 520$ nm), the antinode is located 800 Å from the electrode. At this distance, $W_{\text{TOT}} - W_{\text{NR}} \sim W_0$ (Fig. 2), and nonradiative transfer to the metal electrode is minimized. Figure 12(a) shows the dependence of the rate of energy transfer into the radiative modes that emit through the substrate surface ($W_R^{(\text{surface})}$) as a function of Alq_3 thickness (dashed line), in an OLED with a 400-Å-thick α-NPD layer. As predicted, there is a broad maximum for Alq_3 thicknesses of from 600 to 800 Å, with only a weak dependence on the thickness of the other layers. Since the internal photoluminescence quantum efficiency of Alq_3 (Ref. 17) is $\eta_0 = 0.32 \pm 0.05$, then using Eq. (1) we infer $W_{\text{NR}} \sim 2W_0$ for singlet excitons. The radiative OLED efficiency can now be obtained using Eq. (6). However, in an electrically pumped device, both singlet and triplet excitons are generated, the latter of which do not contribute to the radiative output. Furthermore, a fraction of carriers can pass through the device without forming excitons. Therefore, to obtain η_R, Eq. (6) must be multiplied by the fraction κ of injected carriers that ultimately result in singlet excitons. Assuming κ is a constant independent of Alq_3 thickness, and further, that no additional exciton quenching processes exist, we scale our theoretical predictions to match the experimental measurements, and find $\kappa = 0.05 \pm 0.01$. The resulting value of η_R (solid line) is plotted in Fig. 12(a), together with the experimentally measured values (open circles). Thus, ~12% of singlet excitons (in an OLED with a 500-Å-thick layer of Alq_3) result in a photon emitted through the substrate surface.

The calculations for $W_R^{(\text{surface})}$ assume the ITO refractive index of $n_{\text{ITO}} = 1.8$. By modifying the ITO deposition conditions, it is possible to significantly change its refractive index, which affects the efficiency of radiative coupling. For example, for $n_{\text{ITO}} = 2.2$, η_R increases by approximately 30% in the optimized structure.[18]

A principal figure of merit for an OLED is its power efficiency. The consumed power P increases with the Alq_3 layer thickness due to the concomitant increase in voltage.[22] This is evident in Fig. 12(b), where we plot P (open circles) for the series of OLED's in Fig. 12(a), at $I = 10$ mA/cm^2. We then calculate the power efficiency, $\eta_P^{(\text{surface})}$, using

$$\eta_P^{(\text{surface})} = \eta_R^{(\text{surface})} h\bar{\nu} I L_{h\nu} / qP. \tag{10}$$

Here, $L_{h\nu}$ is the average luminance of an emitted photon, $h\bar{\nu}$ is the average photon energy, and q is the electron charge. For Alq_3 OLED's $L_{h\nu} = 435$ lm/W of optical output power and $h\bar{\nu} = 2.3$ eV. Using Eq. (10) we then find that the maximum power efficiency of 0.7 lm/W is achieved for devices with 500-Å-thick Alq_3 layer [solid circles in Fig. 12(b)].

V. MICROCAVITY EFFECTS IN A STACKED OLED

To demonstrate the general applicability of our theoretical analysis, we apply it to calculating the EL spectra of individual elements of a stacked OLED structure. The SOLED (Fig. 3) consists of green, blue, and red OLED's grown in a vertical sequence on top of a ~1-mm-thick glass substrate with an ITO anode. Ignoring the small refractive index differences between organic layers and the ITO that give rise to only small corrections to our analysis, this complex, fourteen-layer structure represents a device with two coupled microcavities shown in Fig. 3. Reflections from the 1000-Å-thick Mg:Ag cathode and the semitransparent 80-Å-thick Mg:Ag layer form the first microcavity. The second, weaker cavity is formed due to reflections at the semitransparent Mg:Ag layer and the ITO/glass interface.

Our model requires knowledge of the intrinsic radiation spectrum of each element of the stacked OLED. The calculated intrinsic spectra (solid lines) are obtained from the measured $\Theta = 0°$ EL spectra [symbols in Fig. 13(a)] of discrete red, green, and blue devices with layer thicknesses and compositions identical to those used in the composite SOLED. The intrinsic spectra are then used in Eqs. (4) or (5) to obtain the $\Theta = 0°$ EL emission of the compound SOLED with the measured layer thicknesses and refractive indices listed in Fig. 3. We make the approximation that light is generated uniformly throughout the EL layers (i.e., the DCM2:Alq_3, $Alq_2'OPh$, and Alq_3 layers for the red, blue, and green elements, respectively).

In Fig. 13(b), calculated (solid lines) and measured (symbols) $\Theta = 0°$ EL spectra of individual elements of the SOLED are compared.[28] The generally good agreement is apparent. The EL spectrum of the blue OLED is shifted and narrowed relative to its intrinsic spectrum due to the effects of the upper microcavity, while the red EL spectrum is essentially unchanged by the stack, being far from this microcavity resonance. The spectrum of the green OLED shows a shoulder at $\lambda = 500$ nm due to coupling of light into the upper microcavity.

Applying our theoretical model to this SOLED structure, we find that the spectra are insensitive to the thickness variation of any one layer to within $\pm 20\%$, but they are quite sensitive to the change in the thickness of the upper microcavity (Fig. 3). For example, a 10% decrease in the thickness of this microcavity eliminates the spectral peak shift for the blue device, decreases the shift for the green device by 10 nm, while the red device spectrum is only marginally affected. This can be understood by noting that the narrow transmission band of the upper microcavity has a ~50-nm half width with a center wavelength at $\lambda = 500$ nm. Therefore, the emission spectra of the blue and green devices are strongly affected by the position of this resonance, while the spectrum of the red device is sufficiently far from the cavity resonance to be affected by such minor changes in thickness.

For the SOLED of Fig. 3, we also investigated the change in EL emission as a function of Θ by measuring spectra at $\Theta = 30°$ [shown as a solid line in Fig. 13(c) together with $\Theta = 0°$ data]. As expected, only the blue element, being close to the resonance of the upper microcavity, shows a significant variation over this angular range, shifting by 10 nm. The green and red elements exhibit no color shifts, confirming that they are unaffected by cavity resonances in the dielectric stack.

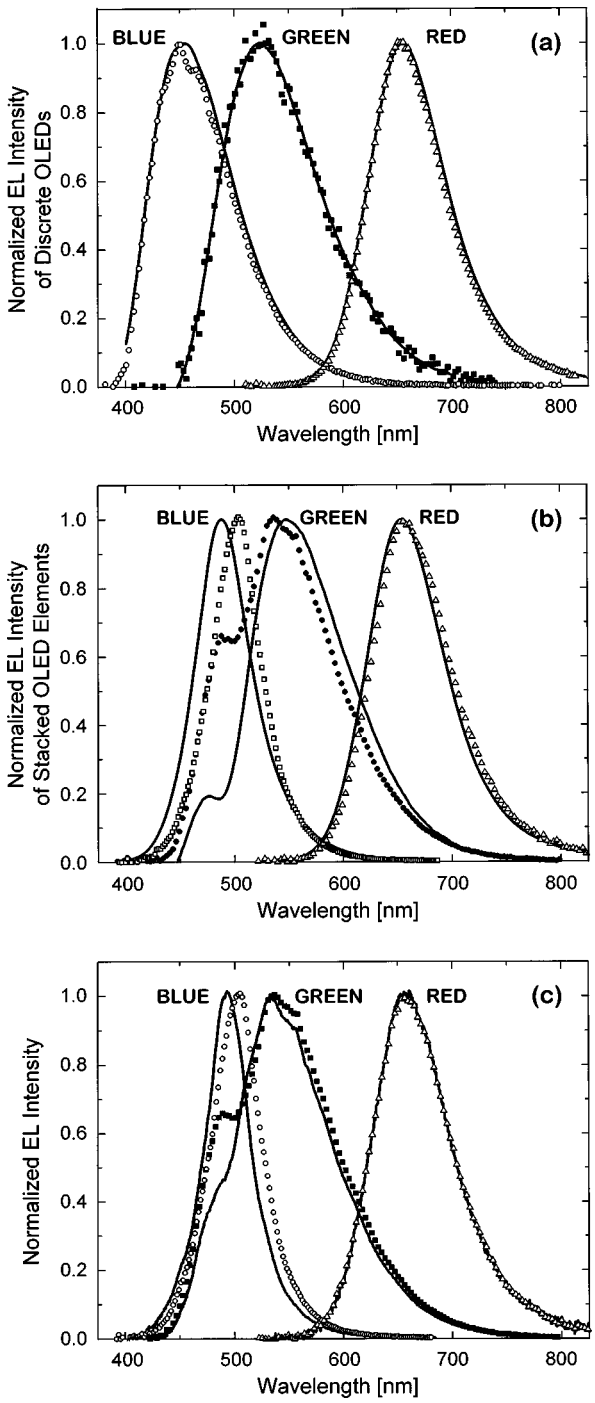

FIG. 13. (a) Intrinsic luminescence spectra (solid line) of 3% DCM2 in Alq_3, Alq_3, and $Alq_2'OPh$, derived from the $\Theta = 0°$ EL spectra of OLED's (symbols) with respective luminescent layers. (b) EL spectra at $\Theta = 0°$ of the red, green, and blue element of a stacked OLED (symbols) with structure shown in Fig. 3. Theoretical fits that utilize intrinsic spectra from (a) are shown as the solid lines. (c) Comparison of EL spectra at $\Theta = 0°$ (symbols) and $\Theta = 30°$ (solid line) of the red, green, and blue elements of the stacked OLED.

Modeling of the complex SOLED structure rigorously tests the reliability of our theoretical treatment. Good agree-

ment with experimental measurements gives us confidence that our theoretical model can be applied as a tool for future OLED design.

VI. CONCLUSION

We presented a comprehensive theoretical analysis that fully describes the behavior of OLED emission, treating both radiative and waveguided modes. Expanding on previous studies, we determined the dependence of the OLED EL spectral intensity and polarization on emission angle, organic layer thickness, and applied voltage. We have shown that by redirecting the edge-emitted light, a significant enhancement in the forward scattered radiative efficiency can be achieved. Due to absorption by the metal electrode, waveguided light is virtually eliminated. Comparing experimental measurements to our theoretical model, we conclude that in electrically pumped Alq_3-based OLED's, the fraction of injected carriers that generate singlet excitons is $5 \pm 1\%$. The radiative emission efficiency of the conventional OLED structure is found to be strongly dependent on the Alq_3 layer thickness, which should be $\sim$700 Å for the highest OLED quantum efficiency, and $\sim$350 Å to maximize its power efficiency.

The versatility and accuracy of the theoretical treatment was demonstrated by modeling the luminescence spectra of individual OLED's in a complex, fourteen-layer stacked OLED structure. By optimizing the SOLED for color saturation in the red, green, and blue spectral bands, the spectral dependence on emission angle was minimized.

The comprehensive understanding of the directionality and polarization of spontaneous emission in layered structures afforded by this study is essential for optimizing the emission characteristics of complex OLED structures as well as organic semiconductor lasers.

ACKNOWLEDGMENTS

We thank E. Bose, D. O'Brien, and M. Baldo for assistance with sample preparation. We also acknowledge DARPA, AFOSR, and Universal Display Corporation for their generous support of this research.

[1] T. Tsutsui, C. Adachi, S. Saito, M. Watanabe, and M. Koishi, Chem. Phys. Lett. **182**, 143 (1991).
[2] A. Dodabalapur, L. J. Rothberg, R. H. Jordan, T. M. Miller, R. E. Slusher, and J. M. Phillips, J. Appl. Phys. **80**, 6954 (1996).
[3] T. Tsutsui, N. Takada, S. Saito, and E. Ogino, Appl. Phys. Lett. **65**, 1868 (1994).
[4] V. Bulović, V. G. Kozlov, V. B. Khalfin, and S. R. Forrest, Science **279**, 553 (1998).
[5] S. Saito, T. Tsutsui, M. Erra, N. Takada, C. Adachi, Y. Hamada, and T. Wakimoto, Proc. SPIE **1910**, 212 (1993).
[6] E. M. Purcell, Phys. Rev. **69**, 681 (1946).
[7] H. Kuhn, J. Chem. Phys. **53**, 101 (1970).
[8] K. H. Drexhage, in *Progress in Optics, Vol. XII*, edited by E. Wolf (North-Holland, Amsterdam, 1974), p. 163.
[9] R. R. Chance, A. Prock, and R. Sibley, *Advances in Chemical Physics*, Vol. 37, edited by S. A. Rice and I. Prigogine (Wiley-Interscience, New York, 1978), p. 1.
[10] G. Björk, S. Machida, Y. Yamamoto, and K. Igeta, Phys. Rev. A **44**, 669 (1991).
[11] D. G. Deppe and C. Lei, J. Appl. Phys. **70**, 3443 (1991).
[12] M. Born and E. Wolf, *Principles of Optics* (Pergamon Press, New York, 1964).
[13] V. Cirmová and D. Neher, J. Appl. Phys. **79**, 3299 (1996).
[14] D. G. Lidzey, M. A. Pate, D. M. Whittaker, D. D. C. Bradley, M. S. Weaver, A. A. Fisher, and M. S. Skolnick, Chem. Phys. Lett. **263**, 655 (1996).
[15] J. Grüner, F. Cacialli, and R. H. Friend, J. Appl. Phys. **80**, 207 (1996).
[16] H. F. Wittmann, J. Grüner, R. H. Friend, G. W. C. Spencer, S. C. Moratti, and A. B. Holmes, Adv. Mater. **7**, 541 (1995).
[17] D. Z. Garbuzov, V. Bulović, P. E. Burrows, and S. R. Forrest, Chem. Phys. Lett. **249**, 433 (1996).
[18] G. Gu, D. Z. Garbuzov, P. E. Burrows, S. Venkatesh, S. R. Forrest, and M. E. Thompson, Opt. Lett. **22**, 396 (1997).
[19] C. W. Tang and S. A. VanSlyke, Appl. Phys. Lett. **51**, 913 (1987).
[20] Z. Shen, P. E. Burrows, V. Bulović, S. R. Forrest, and M. E. Thompson, Science **276**, 2009 (1997).
[21] M. Pope and C. E. Swenberg, *Electronic Processes in Organic Crystals* (Oxford University Press, Oxford, 1982).
[22] P. E. Burrows *et al.*, J. Appl. Phys. **79**, 7991 (1996).
[23] S. Ramo, J. R. Whinnerey, and T. Van Duzer, *Fields and Waves in Communication Electronics* (J. Wiley & Sons, New York, 1984).
[24] V. Bulović, P. Tian, P. E. Burrows, M. Ghokale, S. R. Forrest, and M. E. Thompson, Appl. Phys. Lett. **70**, 2954 (1997).
[25] V. Bulović, A. Shoustikov, M. A. Baldo, E. Bose, V. G. Kozlov, M. E. Thompson, and S. R. Forrest, Chem. Phys. Lett. **287**, 455 (1998).
[26] M. Hiramoto, J. Tani, and M. Yokoyama, Appl. Phys. Lett. **62**, 666 (1993).
[27] H. Kanai, S. Ichinosawa, and Y. Sato, Synth. Met. **91**, 195 (1997).
[28] P. E. Burrows, V. B. Khalfin, G. Gu, and S. R. Forrest, Appl. Phys. Lett. (to be published).